

# 8 Magnetism, Structure and Interactions at the Atomic Scale

V.S. Stepanyuk<sup>1</sup> and W. Hergert<sup>2</sup>

<sup>1</sup> Max Planck Institute of Microstructure Physics, Weinberg 2, 06120 Halle, Germany

<sup>2</sup> Martin-Luther-University Halle-Wittenberg, Department of Physics, Von-Seckendorff-Platz 1, 06120 Halle, Germany

**Abstract.** An efficient scheme is developed to study magnetism and structure as well as interaction between supported particles on the atomic scale. Starting by ab initio calculations of the electronic structure in the framework of density functional theory, interaction potentials for molecular dynamics simulations of metallic nanostructures supported on metallic surfaces are carefully optimized.

The two methods are shortly explained. Examples for the application of the methods are given. Mainly electronic and structural properties of Co nanostructures on Cu(001) and Cu(111) surfaces are investigated.

## 8.1 Introduction

The essence of nanoscience and technology is the ability to understand and manipulate matter at the atomic level. Structures behave differently when their dimensions are reduced to dimensions between 1 and 100 nm. Such structures show novel physical and chemical properties, due to their nanoscopic size.

In the frontier field of nanomagnetism, understanding of the relationship between magnetism and structure plays a central role. During the past few years experimental investigations of metallic nanostructures in the initial stage of heteroepitaxial growth revealed a lot of information which asks for a consistent theoretical explanation. Some important effects experimentally observed recently are:

- Surface alloying is found also for metals immiscible in bulk form (i.e. Co on Cu(001) ). [8.1,8.2]
- Burrowing of Co clusters into Au, Cu and Ag surfaces has been observed. [8.3,8.4]
- It was observed, that the motion of adatoms on top of islands is not the same as on a flat surface. [8.5]
- Fast island decay in homoepitaxial growth was observed by Giesen *et al.* [8.6–8.9]
- By using STM (scanning tunnelling microscope) adsorbate manipulation techniques, it is possible to construct atomic-scale structures on metal surfaces and to study artificially confined quantum systems. [8.10]

To discuss all the effects from theoretical point of view, to get a deep understanding of the underlying physics, it is absolutely necessary to investigate the real structure of the system as well as the electronic and magnetic structure of the nanosystems, because these aspects are strongly interconnected on the atomic scale.

Our combination of the Korringa-Kohn-Rostoker (KKR) Green's function (GF) method with a molecular dynamics (MD) scheme allows us to study the effects mentioned above in detail.

We will discuss the methods briefly. The magnetic properties of metallic nanostructures are discussed. We start from an ideal lattice structure and take into account step by step imperfections, mixing and relaxations. The effect of quantum interference and the implications for long-range interactions and self-organization are discussed next. Finally, we introduce the new concept of mesoscopic misfit and discuss the consequences for strain fields, adatom motion and island decay.

## 8.2 Theoretical Methods

### 8.2.1 Calculation of Electronic Structure

Our calculations are based on the density functional theory and multiple-scattering approach using the Korringa-Kohn-Rostoker Green's function method for low-dimensional systems [8.11]. The basic idea of the method is a hierarchical scheme for the construction of the Green's function of adatoms on a metal surface by means of successive applications of Dyson's equation. We treat the surface as an infinite two-dimensional perturbation of the bulk.

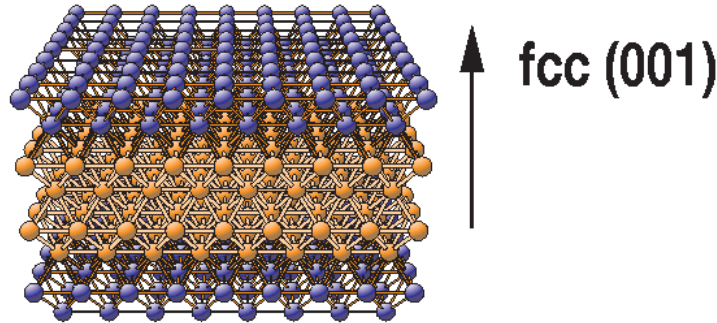


**Fig. 8.1.** Structure to calculate the surface Green's function for the (001) surface of the fcc-structure (blue -decoupled half-crystals, brown - vacuum layers).

For the construction of the ideal surface the nuclear charges of several monolayers are removed, thus creating two half crystals being practically

uncoupled. Taking into account the 2D periodicity of the ideal surface, we calculate the structural Green's function by solving a Dyson equation self-consistently:

$$G_{LL'}^{jj'}(\mathbf{k}_{\parallel}, E) = \mathring{G}_{LL'}^{jj'}(\mathbf{k}_{\parallel}, E) + \sum_{j''L''} \mathring{G}_{LL''}^{jj''}(\mathbf{k}_{\parallel}, E) \Delta t_{L''}^{j''}(E) G_{L''L'}^{j''j'}(\mathbf{k}_{\parallel}, E) \quad (8.1)$$

Here  $\mathring{G}$  is the structural Green's function of the bulk in a  $\mathbf{k}_{\parallel}$ -layer representation ( $j, j'$  - layer indices). The  $\mathbf{k}_{\parallel}$  wave vector belongs to the 2D Brillouin zone.  $\Delta t_L^j(E)$  is the perturbation of the  $t$  matrix to angular momentum  $L = (l, m)$  in the  $j$ -th layer.

The consideration of adsorbate atoms on the surface destroys the translation symmetry. Therefore the Green's function of the adsorbate adatom on the surface has to be calculated in a real space formulation. The structural Green's function of the ideal surface in real space representation is then used as the reference Green's function for the calculation of the adatom-surface system from an algebraic Dyson equation:

$$G_{LL'}^{nn'}(E) = \mathring{G}_{LL'}^{nn'}(E) + \sum_{n''L''} \mathring{G}_{LL''}^{nn''}(E) \Delta t_{L''}^{n''}(E) G_{L''L'}^{n''n'}(E), \quad (8.2)$$

where  $G_{LL'}^{nn'}(E)$  is the energy-dependent structural Green's function matrix and  $\mathring{G}_{LL''}^{nn''}(E)$  the corresponding matrix for the ideal surface, serving as a reference system.  $\Delta t_L^n(E)$  describes the difference in the scattering properties at site  $n$  induced by the existence of the adsorbate atom.

Exchange and correlation effects are included in the local density approximation. The full charge density and the full potential approximation can be used in the calculations. Details of the method and several of its applications can be found elsewhere [8.11].

### 8.2.2 Molecular Dynamics Simulations

In the last years we developed a method which connects the ab initio electronic structure calculations with large scale molecular dynamics simulations. Our approach is based on fitting of the interaction parameters of potentials for molecular dynamic simulations to accurate first-principle calculations of selected cluster-substrate properties, bulk properties and forces acting on adatoms of the system under investigation. [8.12]

To describe metallic clusters on noble metal substrates, many body potentials in the second moment tight-binding approximation are used. [8.13,8.14]

The cohesive energy  $E_{\text{coh}}$  is the sum of the band energy  $E_{\text{B}}$  and the repulsive part  $E_{\text{R}}$

$$E_{\text{coh}} = \sum_i (E_{\text{B}}^i + E_{\text{R}}^i) \quad (8.3)$$

$$E_{\text{B}}^i = - \left( \sum_j \xi_{\alpha\beta}^2 \exp(-2q_{\alpha\beta}(r_{ij}/r_0^{\alpha\beta} - 1)) \right)^{1/2} \quad (8.4)$$

$$E_{\text{R}}^i = \sum_j \left( A_{\alpha\beta}^1 (r_{ij}/r_0^{\alpha\beta} - 1) + A_{\alpha\beta}^0 \right) \exp(-p_{\alpha\beta}(r_{ij}/r_0^{\alpha\beta} - 1)) \quad (8.5)$$

where  $r_{ij}$  represents the distance between the atoms  $i$  and  $j$ , and  $r_0^{\alpha\beta}$  is the first-neighbour distance in the  $\alpha, \beta$  lattice structure, while it is just an adjustable parameter in the case of the cross interaction.  $\xi$  is an effective hopping integral and depends on the material and  $q_{\alpha\beta}$  and  $p_{\alpha\beta}$  describe the dependence of the interaction strength on the relative interatomic distance.

**Table 8.1.** Data used for the fitting of the potential together with the values calculated with the optimized potential. (cohesive energy  $E_c$ , bulk modulus B, elastic constants  $C_{ij}$  from Cleri *et al.* [8.13], first and second neighbour interaction energies  $E_{1,b}^{\text{Co-Co}}$ ,  $E_{2,b}^{\text{Co-Co}}$  from Hoshino *et al.* [8.15] solution energy  $E_{\text{S}}^{\text{Co in Cu}}$  from Drittler *et al.* [8.16] and binding energies of small Co clusters  $E_{1,\text{on Cu}(001)}^{\text{Co-Co}}$ ,  $E_{1,\text{in Cu}}^{\text{Co-Co}}$ ,  $E_{\text{on Cu}(100)}^{\text{trimer}}$ ,  $E_{\text{on Cu}(100)}^{2 \times 2 \text{ island}}$  are calculated using the KKR Green's function method.

	quantity	data	fitted value
Cu (fcc)	$a_{\text{Cu}}$	3.615 Å	3.614 Å
	$E_c$	3.544 eV	3.545 eV
	B	1.42 Mbar	1.42 Mbar
	$C_{11}$	1.76 Mbar	1.76 Mbar
	$C_{12}$	1.25 Mbar	1.25 Mbar
	$C_{44}$	0.82 Mbar	0.82 Mbar
Co	$a_{\text{Co}}$	2.507 Å	2.515 Å
	$E_c$	4.386 eV	4.395 eV
	B	1.948 Mbar	1.989 Mbar
	$C_{11}$	3.195 Mbar	3.337 Mbar
	$C_{12}$	1.661 Mbar	1.426 Mbar
	$C_{13}$	1.021 Mbar	1.178 Mbar
	$C_{33}$	3.736 Mbar	3.665 Mbar
	$C_{44}$	0.824 Mbar	0.646 Mbar
Co-Cu	$E_{\text{S}}^{\text{Co in Cu}}$	0.4 eV	0.38 eV
	$E_{1,b}^{\text{Co-Co}}$	-0.12 eV	-0.18 eV
	$E_{2,b}^{\text{Co-Co}}$	0.03 eV	-0.05 eV
	$E_{1,\text{on Cu}(001)}^{\text{Co-Co}}$	-1.04 eV	-1.04 eV
	$E_{1,\text{in Cu}}^{\text{Co-Co}}$	-0.26 eV	-0.35 eV
	$E_{\text{on Cu}(100)}^{\text{trimer}}$	-2.06 eV	-1.96 eV
	$E_{\text{on Cu}(100)}^{2 \times 2 \text{ island}}$	-3.84 eV	-3.86 eV

We will explain the method for the system Co/Cu(001). Co and Cu are not miscible in bulk form. Therefore the determination of the cross interaction is a problem. A careful fitting to accurate first-principles calculations of selected cluster substrate properties solves the problem. The result is a manageable and inexpensive scheme able to account for structural relaxation and including implicitly magnetic effects, crucial for a realistic determination of interatomic interactions in systems having a magnetic nature. After determination of the Cu-Cu parameters, which are fitted to experimental data only [8.14], the Co-Co and Co-Cu parameters are optimized simultaneously by including in the fit the results of first-principles KKR calculations. To this purpose, we have taken the solution energy of a single Co impurity in bulk Cu  $E_S^{\text{Co in Cu}}$  [8.16], energies of interaction of two Co impurities in Cu bulk [8.15]  $E_{1,b}^{\text{Co-Co}}$ ,  $E_{2,b}^{\text{Co-Co}}$  and binding energies of small supported Co clusters on Cu(001) -  $E_{1,\text{on Cu(001)}}^{\text{Co-Co}}$ ,  $E_{1,\text{in Cu}}$  (terrace position),  $E_{\text{on Cu(100)}}^{\text{trimer}}$ ,  $E_{\text{on Cu(100)}}^{2 \times 2 \text{ island}}$ . The set of data used to define the potential and the corresponding values calculated by means of the optimized potential are given in Table 8.1. The bulk and surface properties are well reproduced.

The method, discussed so far has been further improved. We are able to calculate forces on atoms above the surface on the ab initio level. The forces are also included in the fitting procedure. This gives a further improvement of the potentials used in the MD simulations. It should be mentioned that our method allows also to use only ab initio bulk properties from KKR calculations. Therefore, we can construct ab initio based many-body potentials.

### 8.3 Magnetic Properties of Nanostructures on Metallic Surfaces

Using the KKR Green's function method we have studied the properties of 3d, 4d and 5d adatoms on Ag(001), Pd(001) and Pt(001) systematically. [8.17, 8.18] One central point of investigation was the study of imperfect nanostructures. We have investigated the influence of Ag impurities on the magnetism on small Rh and Ru clusters on the Ag(001) surface. [8.19] The change of the magnetic moments could be explained in the framework of a tight-binding model. Nevertheless it was observed that the magnetism of Rh nanostructures shows some unusual effects. [8.20] An anomalous increase in the magnetic moments of Rh adatoms on the Ag(001) surface with decreasing interatomic distance between atoms was observed, whereas for dimers of other transition metals the opposite behaviour is found.

In this chapter we will discuss some selected results for the real, electronic and magnetic structure of metal nanostructures on noble metal surfaces. We will concentrate our discussion on one special system: Co nanostructures on Cu surfaces. Although a special system is investigated general conclusions can be drawn.

### 8.3.1 Metamagnetic States of 3d Nanostructures on the Cu(001)Surface

The existence of different magnetic states like high spin ferromagnetic (HSF), low spin ferromagnetic (LSF) and antiferromagnetic (AF) states is well known for bulk systems.

A theoretical investigation of Zhou *et al.* [8.21] shows that up to five different magnetic states are found for  $\gamma$  Fe. (LSF, HSF, AF, and two ferromagnetic states). Different theoretical investigations have shown, that energy differences between the magnetic states can be of the order of 1 meV. In such a case magnetic fluctuations can be excited by temperature changes or external fields. Magneto-volume effects play also an important role in the theory of the Invar effect. [8.22]

Lee and Callaway [8.23] have studied the electronic and magnetic properties of free V and Cr clusters. They found that for some atomic spacings as many as four or five magnetic states exists for a  $V_9$  or  $Cr_9$  cluster. The typical low and high spin moments are  $0.33 \mu_B$  and  $2.78 \mu_B$  for the  $V_9$  cluster.

We have calculated the electronic and magnetic properties of small 3d transition metal clusters on the Cu(001) surfaces. Dimers, trimers and tetramers, as given in Fig. 8.2, are investigated. All atoms occupy ideal lattice sites. No relaxation at the surface is taken into account. [8.24, 8.25]

While larger clusters might show a non-collinear structure of the magnetic moments, such a situation is not likely for the clusters studied here. Dimers and tetramers have only one non-equivalent site in the paramagnetic state.

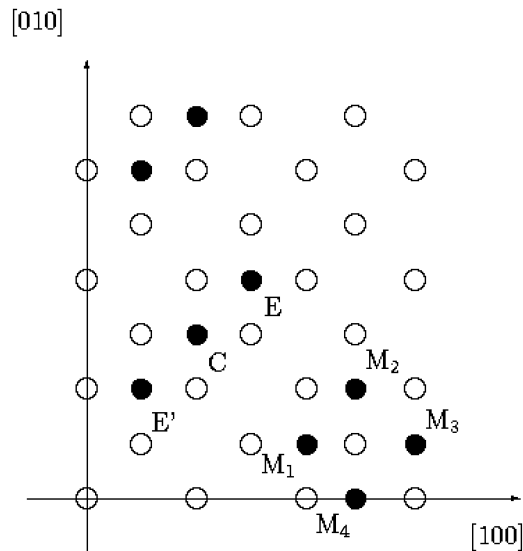


**Fig. 8.2.** Metallic nanostructures (Dimer, trimer and tetramer) on the fcc(001) surface.

The trimers have two non-equivalent sites (C - center, E, E' - edge positions). Ferromagnetic states of the trimers, either low spin (LSF) or high spin (HSF) states, have parallel moments at the sites C and E, E', but the moments have different sign at C and E, E' in the antiferromagnetic state (AF). The atoms at the edge positions (E, E') have the same moment ( $M_E = M_{E'}$ ) for LSF, HSF and AF states. Another possible magnetic state, which is compatible with the chemical symmetry of the system is an antisymmetric (AS) one. The magnetic moment at the central atom of the trimer is zero and the moments at the edge positions have different sign ( $M_E = -M_{E'}$ ).

We concentrate our discussion on the multiplicity of magnetic states to V and Mn. For the single V adatom only a high spin state with a moment of  $3.0 \mu_B$  is obtained. For the  $V_2$  dimer we find both a ferromagnetic and an antiferromagnetic state with moments of  $2.85$  and  $2.58 \mu_B$  respectively. The antiferromagnetic state has the lowest energy being about  $0.2$  eV/atom lower than the ferromagnetic one.

The magnetic moments for all the different magnetic states of the V and Mn trimers are summarized in Table 8.2. All the magnetic states have a lower total energy than the paramagnetic state. The AF state is the ground state of the V trimer. The energy difference between the AF and LSF state in V is about  $8$  meV/atom. The LSF state is more stable than the HSF state. The ground state of the Mn trimer is also the antiferromagnetic state. The energy difference between the ground state and the HSF state is only  $2$  meV/atom. This energy difference corresponds to a temperature difference of  $25$  K. A transition between the two states caused by temperature changes or an external field leads to a change of the total moment of the Mn trimer of  $7.8 \mu_B$ . Such a strong change of the total moment, controlled by an external parameter opens a new field for an experimental proof of the theoretical results.

**Table 8.2.** Magnetic moments (in  $\mu_B$ ) for the atoms of the trimers  $V_3$  and  $Mn_3$  on Cu(001).

state	$V_3$			$Mn_3$		
	$M_E$	$M_C$	$M_{E'}$	$M_E$	$M_C$	$M_{E'}$
HSF	2.85	2.58	2.85	4.03	3.83	4.03
LSF	2.63	1.41	2.63	4.04	0.01	4.04
AF	2.63	-2.02	2.63	3.99	-3.88	3.99
AS	2.62	0.00	-2.62	3.98	0.00	-3.98

We have shown, that metamagnetic behaviour exists in supported clusters. It is shown, that the energy differences between different magnetic states can be small, which can lead to a change of the magnetic state of the cluster by an external parameter. The energy differences between different magnetic

states will strongly depend on the cluster size. Therefore such *ab initio* calculations can help to select interesting systems for experimental investigations.

### 8.3.2 Mixed Co-Cu Clusters on Cu(001)

The magnetic properties of Co nanostructures on Cu substrate can be strongly influenced by Cu atoms. For example, Cu coverages as small as three hundredths of a monolayer drastically affect the magnetization of Co films. [8.26] Experiments and theoretical studies demonstrated that magnetization of mixed clusters of Co and Cu depends on the relative concentration of Co and Cu in a nonobvious way. Quenching of ferromagnetism in Co clusters embedded in copper was reported. [8.27] Calculations by means of our MD method showed that surface alloying is energetically favourable in the case of Co/Cu(001) and mixed Co-Cu clusters are formed in the early stages of heteroepitaxy. Recent experiments [8.2] suggest that mixed Co-Cu clusters indeed exist.

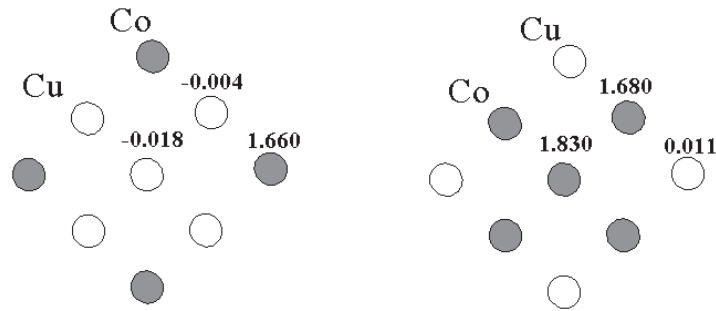


**Fig. 8.3.** Spin polarization of Co-Cu mixed clusters on Cu(001). Magnetic moments in Bohr magnetons are given for all inequivalent site.

We have studied all possible mixed configurations in  $3 \times 3$ -atoms islands on Cu(001) surfaces. [8.28] We observe a small induced moment at the Cu atoms in the island and a decrease of the moments at the Co atoms in comparison with the  $3 \times 3$  Co-island. A stronger reduction of the Co moments is achieved, if the  $\text{Co}_9$  cluster is surrounded by a Cu brim and capped by a Cu cluster. A reduction of 14 % is obtained for the average moment of the  $\text{Co}_9$  cluster. This effect should have a strong influence on the properties of the Co-Cu interface in the early stages of growth. Coating of Co clusters with Cu atoms has been found recently in experiments. [8.4]

### 8.3.3 Effect of Atomic Relaxations on Magnetic Properties of Adatoms and Small Clusters

Possible technological applications of supported magnetic clusters are connected with the magnetic anisotropy energy (MAE), which determines the



orientation of the magnetization of the cluster with respect to the surface. Large MAE barriers can stabilize the magnetization direction in the cluster and a stable magnetic bit can be made. Ab initio calculations have predicted very large MAE and orbital moments for  $3d$ ,  $5d$  adatoms and  $3d$  clusters on Ag(001). [8.29–8.31]

The interplay between magnetism and atomic structure is one of the central issues in physics of new magnetic nanostructures. Performing ab initio and tight-binding calculations we demonstrate the effect of atomic relaxations on the magnetic properties of Co adatoms and Co clusters on the Cu(001) surface. [8.32] We address this problem by calculating magnetic properties of the Co adatom and the  $\text{Co}_9$  cluster on the Cu(100) surface. First, we calculate the effect of relaxations on the spin moment of the Co atom using the KKR Green's function method. (cf. Fig. 8.4)

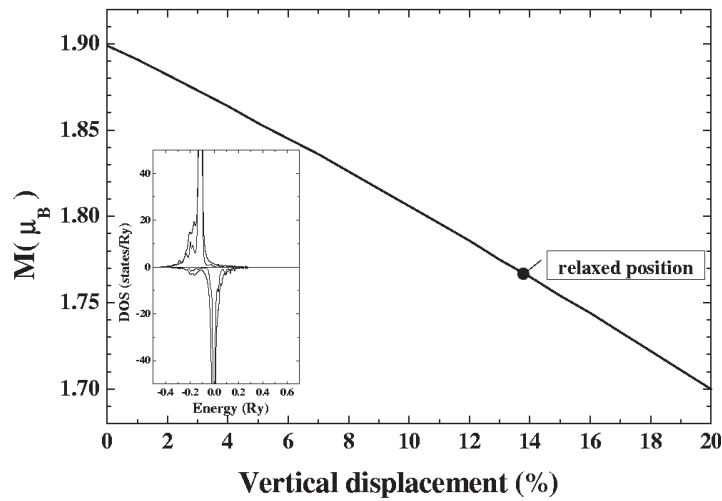


**Fig. 8.4.** The dependence of the spin magnetic moment of the Co adatom on the distance from the Cu substrate. The relaxed position of the adatom is indicated: 0% correspond to Co at a Cu interlayer separation above the Cu surface. The magnetic moments per atom are given in Bohr magnetons. Inset: ab initio (thick line) and TB (thin line) results for the  $d$  component of the local density of states (LDOS) of the Co adatom for unrelaxed position.

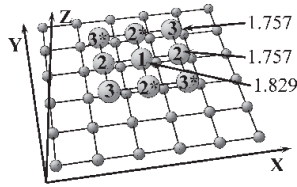
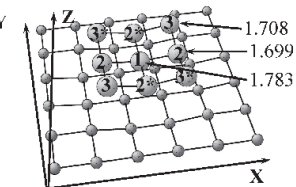
We employ the tight binding electronic Hamiltonian with parameters chosen to fit the KKR local densities of electronic states and the local magnetic moments of Co overlayers and small clusters on Cu(100) to calculate the MAE. To evaluate the MAE the intraatomic spin-orbit coupling is presented by the operator  $\xi \mathbf{L} \cdot \mathbf{s}$  where  $\xi$  is the spin-orbit coupling parameter.

The results for the orbital moments and the MAE of the Co adatoms in the unrelaxed and relaxed positions are presented in Table 8.3. Calculation of

**Table 8.3.** Magnetic orbital moments and magnetic anisotropy energy of a single Co adatom on the Cu(100) surface:  $L_Z^m$  and  $L_X^m$  are the orbital moments for magnetization along the normal Z and in-plane X direction; the electronic part of the magnetic anisotropy energy  $\Delta E$  (meV) is presented.

	Unrelaxed geometry	Relaxed geometry
$L_Z^m$	1.06	0.77
$L_X^m$	1.04	0.80
$\Delta E$	1.70	-0.37

the MAE reveal that for the unrelaxed position above the the surface, out-of plane magnetization for the Co adatom is more stable. The relaxation of the vertical position of the adatom by 14% shortens the first nearest neighbour Co-Cu separation from 2.56 to 2.39 Å and has a drastic effect on MAE. We find that the relaxation of the Co adatom leads to in-plane magnetization.

	Ideal geometry			Relaxed geometry		
						
Atom	$L_Z^m$	$L_X^m$	$\Delta E(X,Z)$	$L_Z^m$	$L_X^m$	$\Delta E(X,Z)$
1	0.11	0.25	-1.48	0.09	0.18	-1.13
2	0.17	0.24	-1.35	0.13	0.19	-1.05
2*	0.17	0.27	-0.87	0.13	0.25	-1.26
3	0.21	0.43	-2.44	0.18	0.39	-2.60
Atom	$L_Z^m$	$L_{X+Y}^m$	$\Delta E(X+Y,Z)$	$L_Z^m$	$L_{X+Y}^m$	$\Delta E(X+Y,Z)$
1	0.11	0.25	-1.47	0.09	0.21	-1.06
2	0.17	0.25	-1.20	0.13	0.20	-1.15
3	0.21	0.40	-2.17	0.18	0.37	-2.38
3*	0.21	0.40	-2.30	0.18	0.35	-2.71

**Fig. 8.5.** Magnetic properties of Co<sub>9</sub> cluster on the Cu(100) surface in unrelaxed and relaxed geometries; spin magnetic moments in Bohr magnetons are shown for each atom in the cluster; orbital magnetic moments and electronic part of the MAE are presented in the table for the normal Z, in-plane X and X + Y directions of the magnetization. For the unrelaxed cluster the the average MAE is -1.74 meV/Co atom for X-direction; for X + Y direction these values are -1.69 meV/Co atom. For the relaxed cluster, the above energies are -1.79 meV/Co atom for X direction and -1.76 meV/Co atom for X + Y direction.

The results for the  $\text{Co}_9$  cluster are presented in Fig. 8.5. We find that the spin moments of atoms of the cluster are close to moments of the Co adatom (see Fig. 8.4) and the Co monolayer ( $1.7 \mu_B$ ). We find that spin and orbital magnetic moments are strongly affected by the relaxation. For example, the orbital moment  $L_X^m$  of the central atom (cf. Fig. 8.5) is reduced by 30 %. This effect is caused by the strong reduction of all first NN Co-Co distances to about 2.41 Å (2.56 Å for the unrelaxed structure). The stability of the in-plane magnetization is reduced by relaxations for the central atom and for atom 2, while it is enhanced for the corner atom and for atom 2\*. For all the atoms in the cluster the MAE is found to be considerably larger than the MAE of the single Co atom in relaxed geometry.

For both, the relaxed and unrelaxed  $\text{Co}_9$  cluster, the magnetization along  $X$  is slightly more stable than along  $X + Y$ . However, MAE from particular atoms have an inhomogeneous distribution and possibility of noncollinear magnetization cannot be ruled out.

## 8.4 Quantum Interference and Interatomic Interactions

Surface-state electrons on the (111) surfaces of noble metals form a two-dimensional (2D) nearly free electron gas. Such states are confined in a narrow layer at the surface. An electron in such a state *runs* along the surface, much like a 2D plane wave. The quantum interference between the electron wave travelling towards the scattering defect and the backscattered one leads to standing waves in the electronic local density of states (LDOS) around

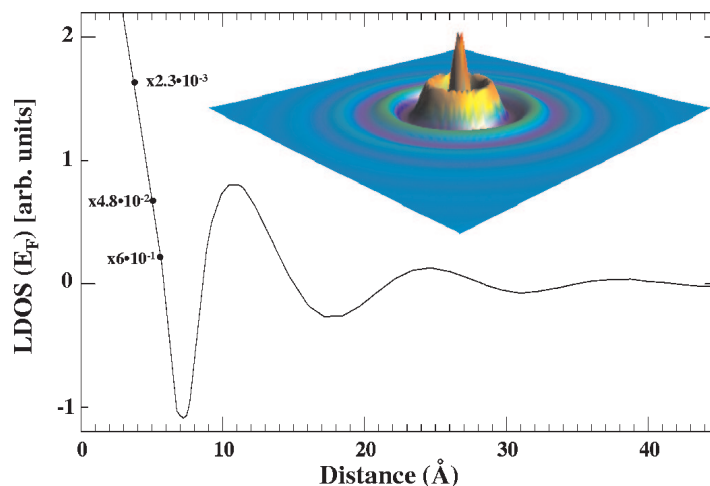


**Fig. 8.6.** Calculated standing waves in the LDOS around single Co atom on Cu(111).

the defect. [8.33] These standing waves are the energy-resolved Friedel oscillations. The scanning tunnelling microscope (STM) images taken at low bias directly reflect the oscillations in the LDOS close to  $E_F$ .

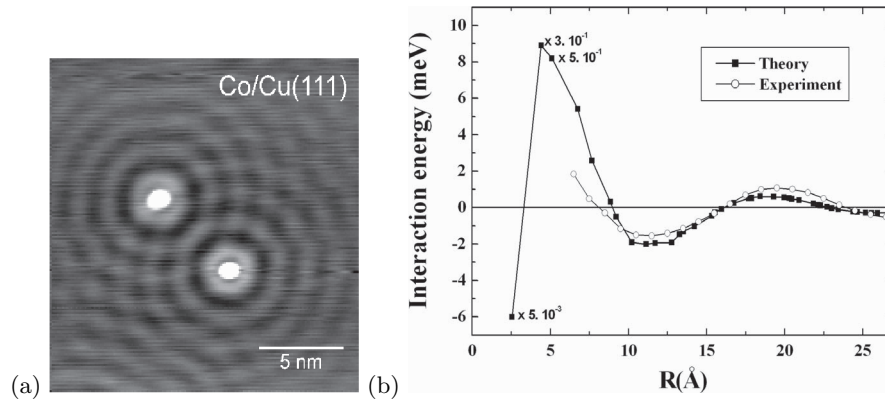


**Fig. 8.7.** (a) Constant current STM image of two Co adatoms on Cu(111) which interact via the standing waves ( $I = 2nA$ ,  $V = -50mV$ ,  $T = 6K$ ); b) Experimental and calculated interaction energies between two Co adatoms on Cu(111).

We will discuss our recent ab initio studies of long-range adsorbate interactions caused by the quantum interference of surface-state electrons. [8.35]

While we concentrate on a particular system, Co adatoms on Cu(111), our results are of general significance because they show that the quantum interference on metal surfaces can strongly affect the growth process of the transition-metal nanostructures.

Our calculation for the Cu(111) surface gives a surface-state Fermi wavelength  $\lambda_F = 29 \text{ \AA}$ . The scattering of surface state electrons by Co atoms leads to quantum interference patterns around the adsorbate. Figure 8.6 shows the calculated LDOS at  $E_F$  displaying the  $\lambda_F/2 \approx 15 \text{ \AA}$  period oscillations. The concentric rings surrounding the the Co adatom (cf. Fig. 8.6, inset) are standing waves due to the quantum interference.

Now we turn to the discussion of the long-range interactions between Co adatoms on Cu(111). An example of a STM image of two Co adatoms at a distance of about  $60 \text{ \AA}$  from each other is shown in Fig. 8.7(a). [8.36] One can see that the atoms share LDOS oscillations with each other. Thus, the adsorbates should interact via Friedel oscillations. The experimental results and calculations (cf. [8.35]) for the interaction energies are presented in Fig. 8.7(b) and they show that the interaction energy is oscillatory with a period of about  $15 \text{ \AA}$ . The ab initio results are in good quantitative agreement with experiment.

The long-range interactions caused by the quantum interference provide a mechanism which leads to self-assembly of one-dimensional structures on Cu(111). (cf. [8.35])

## 8.5 Strain and Stress on the Mesoscale

### 8.5.1 The Concept of Mesoscopic Misfit

If some material is grown on a substrate with a different bond length the lattice mismatch at the interface leads to strain fields. Strain can be relieved through the introduction of defects in the atomic structure, such as dislocations, or by an atomic rearrangement. Usually strain relaxations are predicted on the basis of the macroscopic lattice mismatch between the two materials. However, if the deposited system is of mesoscopic size of several 100 atoms, its intrinsic bond lengths are different from the bond length in the bulk materials. For the Co/Cu(001) interface the *macroscopic* mismatch  $m_0$  between Co and Cu defined as  $m_0 = (a_{\text{Cu}} - a_{\text{Co}})/a_{\text{Cu}}$  ( $a_{\text{Cu}}$  and  $a_{\text{Co}}$  are the lattice constants) is only  $\approx 2\%$ . Several recent experiments have suggested that strain relaxations for submonolayer coverage [8.37] or even for a few monolayers [8.38] cannot be explained by the macroscopic misfit between bulk materials.

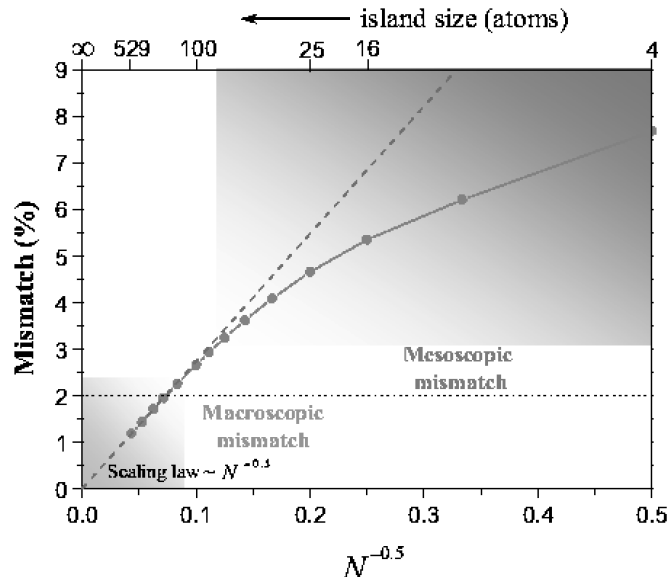


**Fig. 8.8.** Size-dependent mismatch  $m = (r_b^{\text{Cu}} - r^{\text{Co}})/r_b^{\text{Cu}}$  for the Co square islands on Cu(001) ( $r_b^{\text{Cu}}$  - first bond length for Cu bulk;  $r^{\text{Co}}$  - average bond length in Co islands).

In order to get a deeper insight into the local strain relaxations on an atomic scale, the equilibrium geometries of plane square Co islands of different sizes (up to 600 atoms) on Cu(001) are calculated by computing the forces at each atomic site and relaxing the geometry of islands and the substrate atoms using our many-body potentials fitted to ab initio results. [8.39]

In Fig. 8.8 we show the change in the mismatch with the size of Co islands. It is seen, that the *mesoscopic* mismatch between small Co islands and the substrate is considerably larger than the mismatch calculated from the lattice constants of the two materials. Only for Co islands incorporating more than 200 atoms the local strain can be described by the macroscopic mismatch. We found that both the mesoscopic and macroscopic mismatch depend on the size of the islands and for islands larger than 60 atoms mismatch scales like  $N^{-0.5}$  ( $N$  - number of atoms in islands). Such scaling behaviour is determined by the relaxations of the edge atoms of the islands whose number changes as  $\sqrt{N}$ . One very fundamental issue predicted by these results is the possible strong impact of the size dependent mismatch on the local strain field. The substrate can dynamically respond to the growth of islands and can exhibit a strong inhomogeneous strain distribution during the growth process.

### 8.5.2 Strain and Adatom Motion on Mesoscopic Islands

The mesoscopic mismatch and mesoscopic strain depend strongly on the size of the clusters. Therefore we expect that also the barriers for hopping diffusion depend on the size of the clusters. The calculations show, that the barriers for hopping on the small Co islands (16-50 atoms) are found to be about  $\approx 20\%$  lower than those on the large islands (100-500 atoms) (cf. Fig. 8.9). The diffusivity  $D$  is related to the hopping rate of single adatoms by  $D = D_0 \cdot \exp(-E_d/kT)$ , where  $E_d$  is the energy barrier for hopping,  $D_0$  is the prefactor. We found that  $D_0$  is nearly the same for all islands, therefore the diffusion coefficient  $D$  on small Co islands at room temperature is found to be about two orders of magnitude larger than that on large Co islands. [8.40]

### 8.5.3 Mesoscopic Relaxation in Homoepitaxial Growth

Up to now we have discussed strain effects in the heterogeneous system Co on Cu(100). The investigations suggest, that such strain effects should play also an important role in homoepitaxy. But only recently strain effects in homoepitaxy have been discussed in the framework of the concept of mesoscopic mismatch. [8.41, 8.42]

Motivated by the experiments of Giesen *et al.* [8.6–8.9] we concentrate on double layer Cu islands on Cu(111). We reveal that islands and substrate atoms exhibit unexpected strong relaxations.

Now we turn to the discussion of the effect of mesoscopic mismatch in double layers of Cu islands on Cu(111). In this case, the scenario of mesoscopic relaxations is more complicated compared to the flat substrate. Both

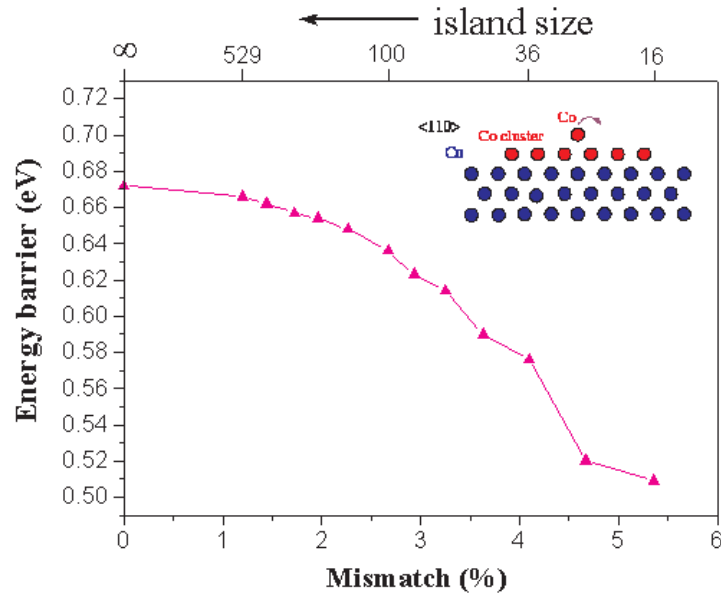


**Fig. 8.9.** Strain dependence of energy barrier for hopping diffusion on top of Co square islands. Since the strain depends on island size, the activation barrier for diffusion depends also on island size (see upper horizontal scale).

the upper and the lower islands exhibit strain relaxations. There are two kinds of step edges: (100) microfaceted step A and (111) microfaceted step B. Due to the relaxation of the edge atoms, the average bond lengths near the island edges at both A and B steps are reduced compared to the center. Therefore, we expect that the mesoscopic mismatch between the upper island and the lower island depends on the distance between the edges and may be different for the step A and the step B. For example, our calculations for a Cu dimer for different positions on the  $\text{Cu}_{271}$  island reveal that when the dimer approaches the edge of the island, mismatch between the dimer and the island changes abruptly and differently for A and B steps. These results suggest that the shape of double layer islands and atomic relaxations in islands and the substrate underneath may depend on the distance between the edges of islands. To prove this, we perform calculations for the double layer Cu island when a close contact between the edges occurs. Results shown in Fig. 8.10 reveal that the atoms at the edge of the lower island and the substrate underneath are pushed up, while atoms of the upper island and the substrate under the large island are pushed down. The strain relief at the edge of islands and in the substrate leads to the shape variation in islands as they approach the edge. We believe that a strongly inhomogeneous displacement pattern in the islands and in the substrate can affect the interlayer mass transport at the edge.

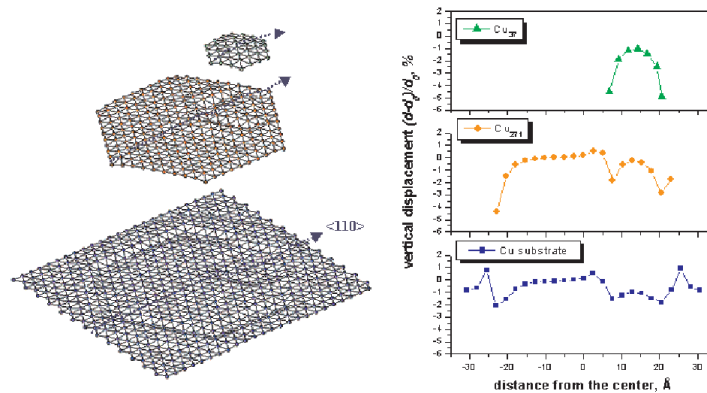


**Fig. 8.10.** The shape of the double layer Cu island and the substrate for a close contact between the island edges. The vertical displacement of Cu atoms in the upper and the lower islands, and in the substrate are shown for  $\langle 110 \rangle$  direction.

### Acknowledgements

We are grateful to J. Kirschner, Š. Pick, A.N. Baranov, P. Bruno, and K. Kern for their contributions to our investigations, helpful suggestions and stimulating discussions.

### References

- [8.1] J. Fassbender, R. Allenspach, and U. Düring, *Surf. Sci* **383**, L742 (1997).
- [8.2] F. Nouvertne, G. Güntherodt, R. Pentcheva, M. Scheffler, *Phys. Rev. B* **60**, 14382 (1999).
- [8.3] S. Padovani, F. Scheurer, and J.P. Bucher, *Europhys. Lett.* **45**, 327 (1999).
- [8.4] C.G. Zimmermann, M. Yeadon, K. Nordlund, J.M. Gibson and R.S. Averback, *Phys. Rev. Lett.* **83**, 1163 (1999).
- [8.5] S.C. Wang and G. Ehrlich, *Phys. Rev. Lett.* **67**, 2509 (1991).
- [8.6] M. Giesen, G. Schulze Icking-Konert, and H. Ibach, *Phys. Rev. Lett.* **80**, 552 (1998).
- [8.7] M. Giesen, G. Schulze Icking-Konert, and H. Ibach, *Phys. Rev. Lett.* **82**, 3101 (1999).
- [8.8] M. Giesen, and H. Ibach, *Surf. Sci. Lett.* **464**, L697 (2000).
- [8.9] M. Giesen, *Prog. Surf. Sci.* **68**, 1 (2001).
- [8.10] M.F. Crommie, *J. Electron Spectrosc. Relat. Phenom.* **109**, 1 (2000); S. Crampin and O.R. Bryant, *Phys. Rev. B* **54**, R17367 (1996).
- [8.11] V.S. Stepanyuk, W. Hergert, R. Zeller, and P.H. Dederichs, *Phys. Rev. B* **53**, 2121 (1996); V.S. Stepanyuk, W. Hergert, P. Rennert, K. Wildberger, R. Zeller and P.H. Dederichs, *Phys. Rev. B* **59**, 1681 (1999); K. Wildberger, V.S. Stepanyuk, P. Lang, R. Zeller, and P.H. Dederichs, *Phys. Rev. Lett.* **75**, 509 (1995); K. Wildberger, P.H. Dederichs, P. Lang, V.S. Stepanyuk, and R. Zeller, *Research Report, Berichte des Forschungszentrum Jülich*, No **3022**, ISSN 0944-2952 (1995).



- [8.12] N.A. Levanov, V.S. Stepanyuk, W. Hergert, D.I. Bazhanov, P.H. Dederichs, A. Katsnelson, and C. Massobrio Phys. Rev. B **61**, 2230 (2000).
- [8.13] V. Rosato, B. Guillope, and B. Legrand, Philos. Mag. A **59**, 321 (1989).
- [8.14] F. Cleri and V. Rosato, Phys. Rev. B **48**, 22 (1993).
- [8.15] T. Hoshino, W. Schweika, R. Zeller, and P.H. Dederichs, Phys. Rev. B **47**, 5106 (1993).
- [8.16] B. Drittler, M. Weinert, R. Zeller, and P.H. Dederichs, Phys. Rev. B **39**, 930(1989).
- [8.17] V.S. Stepanyuk, W. Hergert, P. Rennert, K. Wildberger, R. Zeller, and P.H. Dederichs, Phys. Rev. B **54**, 14121 (1996).
- [8.18] V.S. Stepanyuk, W. Hergert, K. Wildberger, R. Zeller, and P.H. Dederichs, Phys. Rev. B **53**, 2121 (1996).
- [8.19] V.S. Stepanyuk, W. Hergert, P. Rennert, K. Wildberger, R. Zeller, and P.H. Dederichs, Phys. Rev. B **59**, 1681 (1996).
- [8.20] V.S. Stepanyuk, W. Hergert, P. Rennert, J. Izquierdo, A. Vega, and L.C. Balbás, Phys. Rev. B **57**, R14020 (1998).
- [8.21] Yu-mei Zhou, Nuen-qing Zhang, Lie-ping Zhong, and Ding-sheng Wang, J. Magn. Magn. Mater. **145**, L237 (1995).
- [8.22] E.F. Wassermann, Journal of Mag. Mag. Mat. **100**, 346 (1991).
- [8.23] Keeyung Lee and J. Callaway, Phys. Rev. B **48**, 15358 (1993); Keeyung Lee and J. Callaway, Phys. Rev. B **49**, 13906 (1993).
- [8.24] V.S. Stepanyuk, W. Hergert, P. Rennert, K. Wildberger, R. Zeller, P.H. Dederichs, Solid State Commun. **101**, 559 (1997).
- [8.25] V.S. Stepanyuk, W. Hergert, K. Wildberger, S. Najak, P. Jena, Surf. Sci. Lett. **384**, L892 (1997).
- [8.26] W. Weber, C.H. Back, A. Bischof, D. Pescia, and R. Allenspach, Nature (London) **374**,788 (1995).
- [8.27] D.A. Eastham, Y. Qiang, T.H. Maddock, J. Kraft, J.-P. Schille, G.S. Thompson, H. Haberland, J. Phys.: Condensed Matter **9**, L497 (1997).
- [8.28] V.S. Stepanyuk, A.N. Baranov, D.I. Bazhanov, W. Hergert, A.A. Katsnelson, Surface Sci. **482-485**, 1045 (2001).
- [8.29] P. Gambardella,, S. Rusponi, M. Veronese, S.S. Dhesi, C. Grazioli, A. Dallmeyer, I. Cabria, R. Zeller, P.H. Dederichs, K. Kern,C. Carbone, and H. Brune, Science **300**, 1130 (2003).
- [8.30] B. Lazarovits, L. Szunyough, and P. wWeinberger, Phys. Rev. B **65**, 10444 (2002).
- [8.31] B. Nonas, I. Cabria, R. Zeller, P.H. Dederichs, T. Huhne, and H. Ebert, Phys. Rev. Lett. **86**, 2146 (2001).
- [8.32] Š. Pick, V.S. Stepanyuk, A.N. Baranov, W. Hergert, and P. Bruno, Phys. Rev. B **68**, 104410 (2003).
- [8.33] S. Crampin, J. Elect. Spectr. Rel. Phenom. **109**, 51 (2000).
- [8.34] P. Hyltdgaard, and M. Persson, J. Phys: Cond. Matter. **12**, L13 (2000).
- [8.35] V.S. Stepanyuk, A.N. Baranov, D.V. Tsivlin, W. Hergert, P. Bruno, N. Knorr, M.A. Schneider, and K. Kern, Phys. Rev. B **68**, xxxx (2003).
- [8.36] N. Knorr, H. Brune, M. Epple, A. Hirstein, M.A. Schneider, and K. Kern, Phys. Rev. B **65**, 115420 (2002).
- [8.37] D. Sander, R. Skomski, C. Schmidhals, A. Enders, and J. Kirschner, Phys. Rev. Lett. **77**, 2566 1996.
- [8.38] A. Grossmann, W. Erley, J.B. Hannon, and H. Ibach, Phys. Rev. Lett. **77**, 127 1996.

- [8.39] V.S. Stepanyuk, D.I. Bazhanov, A.N.N. Baranov, W. Hergert, P.H. Dederichs, J. Kirschner, Phys. Rev. B **62**, 15398 (2000).
- [8.40] V.S. Stepanyuk, D.I. Bazhanov, W. Hergert, J. Kirschner, Phys. Rev. B **63**, 153406 (2001).
- [8.41] O.V. Lysenko, V.S. Stepanyuk, W. Hergert, and J. Kirschner Phys. Rev. Lett. **89**, 126102 (2002).
- [8.42] O.V. Lysenko, V.S. Stepanyuk, W. Hergert, and J. Kirschner Phys. Rev. B **68**, 033409 (2003).